Regular Article

PHYSICAL CHEMISTRY RESEARCH
Published by the
Iranian Chemical Society
www.physchemres.org
info@physchemres.org

Phys. Chem. Res., *Vol. 7, No. 2, 395-401, June 2019*
DOI: 10.22036/pcr.2019.151365.1546

Fe Lauded TiO_2 Nanoparticles Synthesized by Sol-gel Precursors

M. Farahmandjou[a],* and S. Behrouzinia[b]

[a]*Departments of Physics, Varamin Pishva Branch, Islamis Azad University, Varamin, Iran*

[b]*Laser and Optic Research School, Nuclear Science and Technology Research School, Atomic Energy Organization of Iran, Tehran, Iran*

(Received 6 October 2018, Accepted 9 April 2019)

The pure and 2% Fe doped TiO_2 nanoparticles were synthesized using simple sol-gel method involving an ethanol solvent in the presence of ethylene glycol (EG) as the stabilizer. The physicochemical properties were investigated by field emission scanning electron microscopy (FESEM), X-ray diffraction (XRD), electron dispersive spectroscopy (EDS), diffuse reflectance spectrum (DRS) and photolumincense (PL) analyses. XRD analysis showed the tetragonal anatase structure in presence of Fe doping. The size of the nanoparticles (NPs) decreased to 29 nm by adding Fe content with less agglomeration. PL analysis showed that the intensity of photoluminescence decreases for the doped sample suggesting a decrease in recombination of the electron-holes pair. The UV-DRS analysis indicated that the band gape energy decreases to 3 eV for Fe doped TiO_2 nanoparticles.

Keywords: FESEM, TiO_2 nanoparticles, Fe content, Solgel synthesis

INTRODUCTION

Electron transport in nanoparticles (NPs) causes to different morphological, optical, electrical and magnetic properties for NPs compared to their bulk counterparts [1-10]. Titanium dioxide (TiO_2) is one of the most nanomaterials, because of its stability, ubiquity, non toxicity and none corrosively [11-14]. Depending on the crystalline structure, morphology and crystallite size, TiO_2 is used in different applications, such as electronic devices, solar cells, fine ceramics, transparent conductivity and photo catalytic reactions [15,16]. Recently, many TiO_2 modification procedures have successfully shifted the photocatalytic activity of TiO_2 from the UV region to visible light region, leading to an enhanced photocatalytic activity as a consequence of more complete utilization of solar energy. Narrowing the band gap of TiO_2 can be acquired by doping TiO_2 with various transition metal ions [17]. Various transition metal ions, such as Fe, Co, Zn and V have been introduced for doping TiO_2 to induce a red shift for TiO_2 absorption spectrum and the enhancement of photocatalytic activity [11,12]. Among various metal ions, doping TiO_2 with Fe^{3+} has been widely investigated [18]. Several synthesis methods of TiO_2 have been proposed in the literature including sol-gel [19], flame spray pyrolysis [20] and precipitation [21]. A well-known method for preparing metal ion doping of TiO_2 is based on the sol-gel method via hydrolysis mechanism. In the present work, we synthesize Fe-doped TiO_2 by a new sol-gel precursor while the post annealing of the samples is at 600 °C. The prepared samples are characterized by XRD, SEM, DRS and PL analyses to study the structural, optical and morphological properties.

MATERIALS AND METHODS

Pure and Fe-doped TiO_2 NPs were synthesized using the sol-gel method. In order to synthesize pure TiO_2, at first, $TiCl_4$ precursor was dissolved in pure ethanol using a magnetic stirrer at room temperature. 2 ml Acetic acid was added to the solution, and then the temperature was elevated to 80 °C. 2 ml EG stabilizer was then added at this

*Corresponding author. E-mail: farahamndjou@iauvaramin.ac.ir

temperature. The solution was completely evaporated, and then dried. The product was incubated at 600 °C for 4 h. Fe-doped TiO_2 NPs were synthesized with a method similar to the one used for the preparation of the pure TiO_2 sample adopted with the $FeSO_4$ precursor. The characterization of the samples was carried out in order to study the effect of the Fe doping on the TiO_2 matrix. Structural analysis was performed using the X-ray diffractometer (XRD) and data was recorded with 2θ in the range of 4°-85° using X-Pert Pro MPD, Cu-Kα (λ = 1.5406 Å) radiation. The morphology of the samples was identified using the field emission scanning electron microscope (FESEM) model KYKY-EM3200, 25 kV. Examination of the optical properties was carried out by diffuse reflection spectroscopy (DRS) model Avaspec-2048-TEC to determine the band gap energy of the samples. Photoluminescence studies were carried out by PL spectroscopy, model Avaspec 2048 TEC, at room temperature.

RESULTS AND DISCUSSION

XRD Spectra

Figure 1 shows the XRD analysis of the un-doped and Fe-doped TiO_2 nanocrystals annealed at 600 °C for 4 h. The XRD peaks show the anatase phase with (101), (103), (004), (112), (200), (105), (211), (204), (116), (220), (215) and (031) planes [22,23]. The peak of the rutile phase at the angle of 27.50 is represented as (110) plane. These patterns did not show any change in the tetragonal structure of the anatase TiO_2 nanocrystals despite containing impurity. These results indicate the probability of some Fe^{3+} ions being replaced in the crystal framework of TiO_2 due to their similar radii (a_{Ti}^{4+} = 0.68 Å, a_{Fe}^{3+} = 0.64 Å). The mean crystallite size for pure and Fe-doped TiO_2 samples was calculated using the Debye-Scherrer formula [24] as follows:

$$D = \frac{0.9\lambda}{\beta\cos\theta} \quad (1)$$

where λ is the wavelength of the x-ray used (λ = 1.5060 Å), β is the full width at half maximum (FWHM), and θ is the angle between the incident and the scattered x-ray (Bragg angle). It can be concluded that the crystallite size decreased with the Fe content and the particle size was estimated to be 39 nm and 29 nm for pure and 2% Fe-doped TiO_2, respectively, in agreement with the results previously reported [22,23].

FESEM Analysis

Figure 2 shows the FESEM morphology of the pure (Fig. 2A) and Fe-doped TiO_2 (Fig. 2B) samples. As shown in Fig. 2B, increasing the iron content to 2% reduces the homogeneity and distribution of the particles. A decrease in the size of the particles, for pure and 2% Fe-doped TiO_2 was estimated by the XRD analysis. This causes the agglomeration of NPs, which must be controlled and corrected by using appropriate EG surfactants [25,26]. It is observed that in samples prepared with TTIP precursor, the morphology of the Fe doped TiO_2 nanoparticles is improved [23].

UV-Vis DRS

The band gap and wavelength of absorption were studied using UV-Vis diffuse reflectance spectrum (DRS) for both pure and 2% Fe-doped TiO_2. As shown in Fig. 3, the absorbance peak for doped sample shifted toward longer wavelengths, known as the red shift. This could be due to the reduction in the band gap energy. The indirect band gap energy (E_g) of the NPs has been estimated from the UV-DRS measurements [27], and the F(R) value is calculated from the following equation: $F(R) = (1-R)^2/2R$, where F(R) is the Kubelka-Munk function and R is the percentage reflectance. The indirect band gap was calculated from their reflectance spectra by extrapolating the linear portion of the $[F(R)hy]^{1/2}$ *vs.* E_g plot to F(R) = 0, where the intercept value represents the band gap energy, as shown in Fig. 3. It can be seen that as the Fe concentration increases in TiO_2 to 2%, the band gap energy decreases from 3.52 eV to 3 eV.

PL Activity

Figure 4 shows the photoluminescence of the pure and 2% Fe-doped TiO_2 NPs with an excitation wavelength of 342 nm. The high-energy peaks can be the result of band edge luminescence of the TiO_2 particles, while lower energy peaks/shoulders are induced by the presence of oxygen vacancies. As shown in Fig. 4, the intensity of photoluminescence decreases for doped sample suggesting a

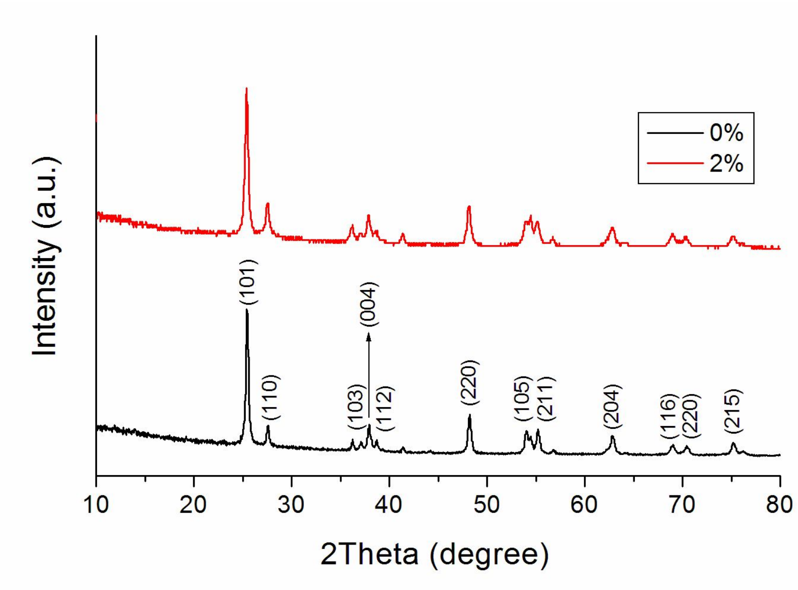

Fig. 1. XRD spectra of pure and 2% Fe-doped TiO_2 nanocrystals.

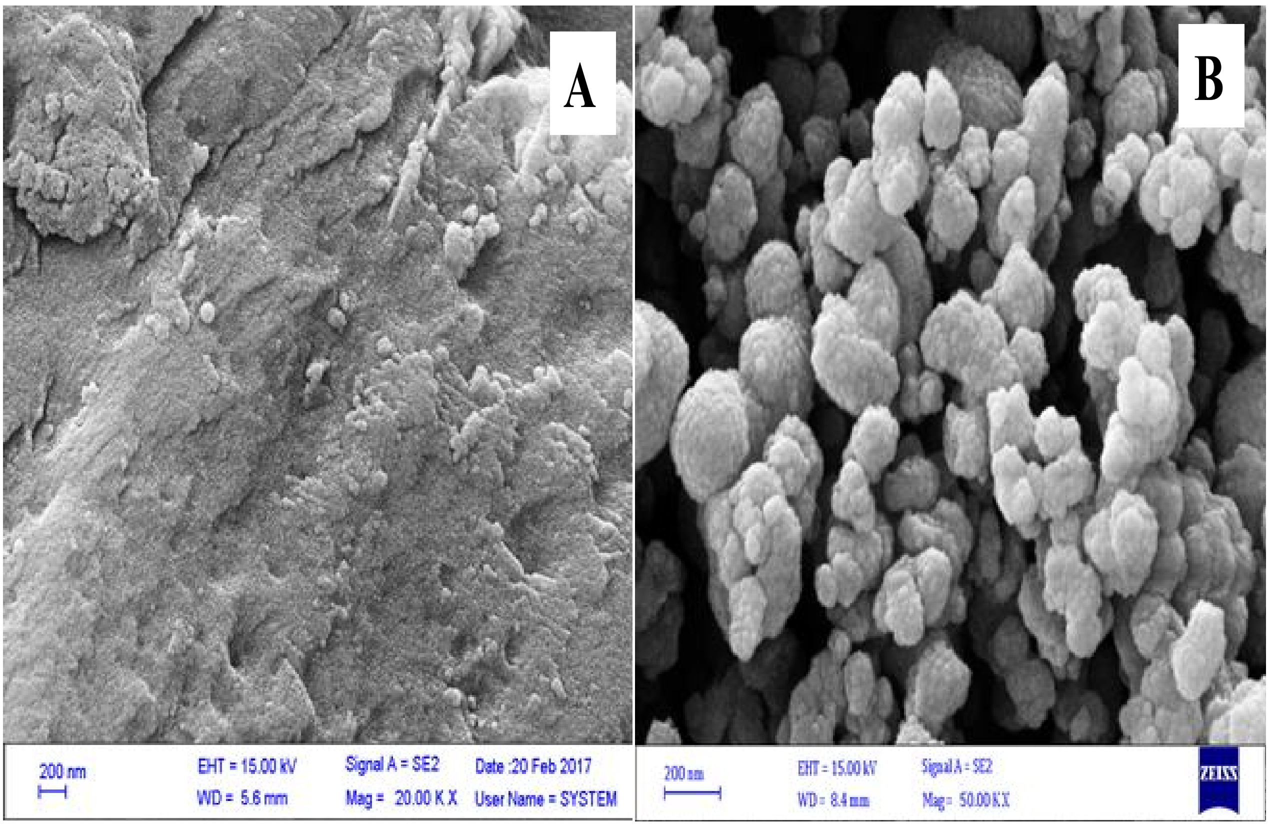

Fig. 2. FESEM images of (A) pure and (B) 2% Fe-doped TiO_2 samples.

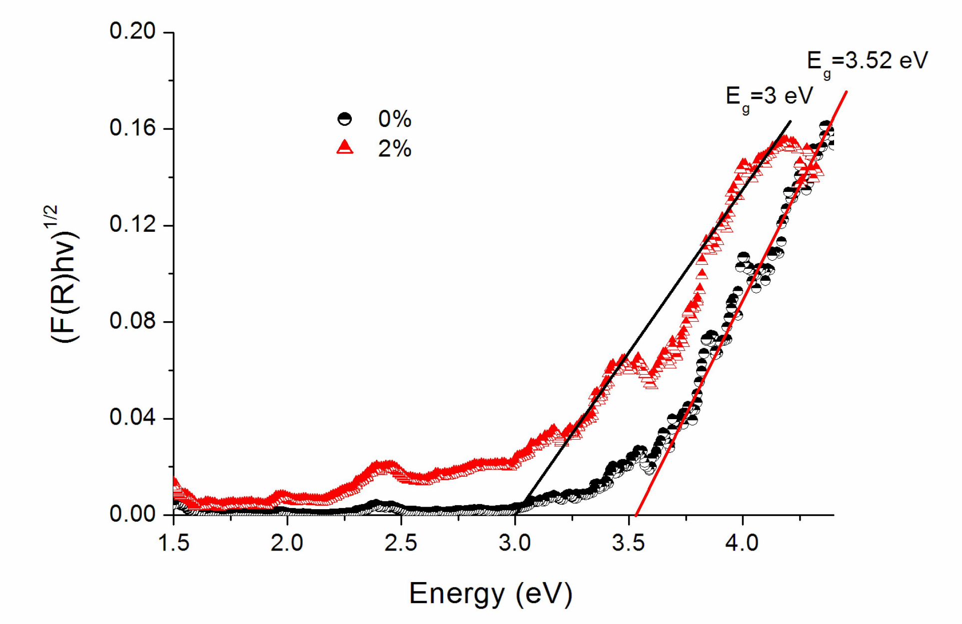

Fig. 3. Plot of $[F(R)h\nu]^{1/2}$ *vs*. E($h\nu$) energy of the pure and 2% Fe-doped TiO_2 samples.

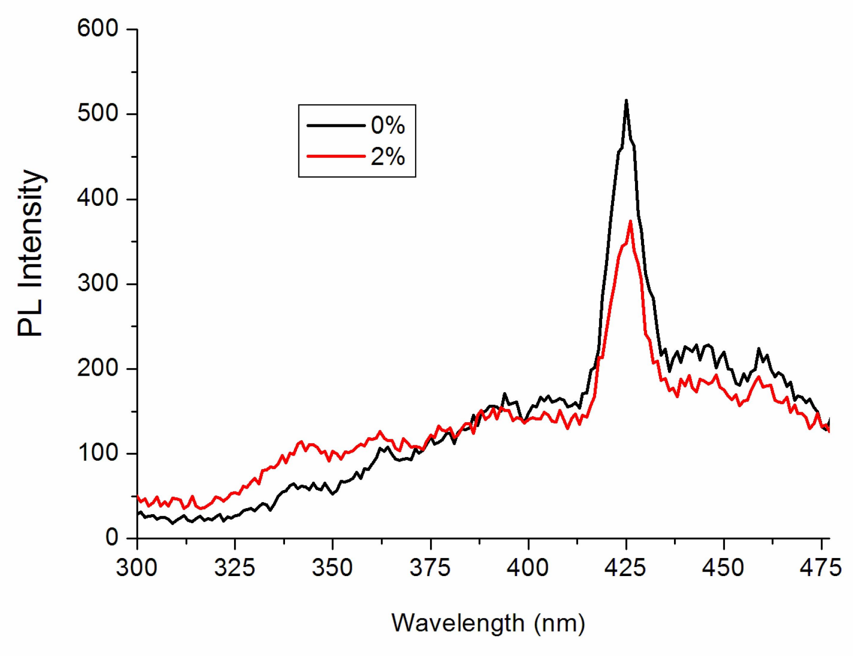

Fig. 4. Photoluminescence (PL) spectroscopy of pure and Fe-doped TiO_2 samples.

decrease in recombination of the electron-holes pair. These results indicate that Fe dopant is entered into the TiO_2 lattice, while in the previous studies [22,23] the samples prepared by the TTIP precursor, the PL intensity increased by Fe impurity and the recombination of electron-hole increased. In fact, the generated photo-induced electron

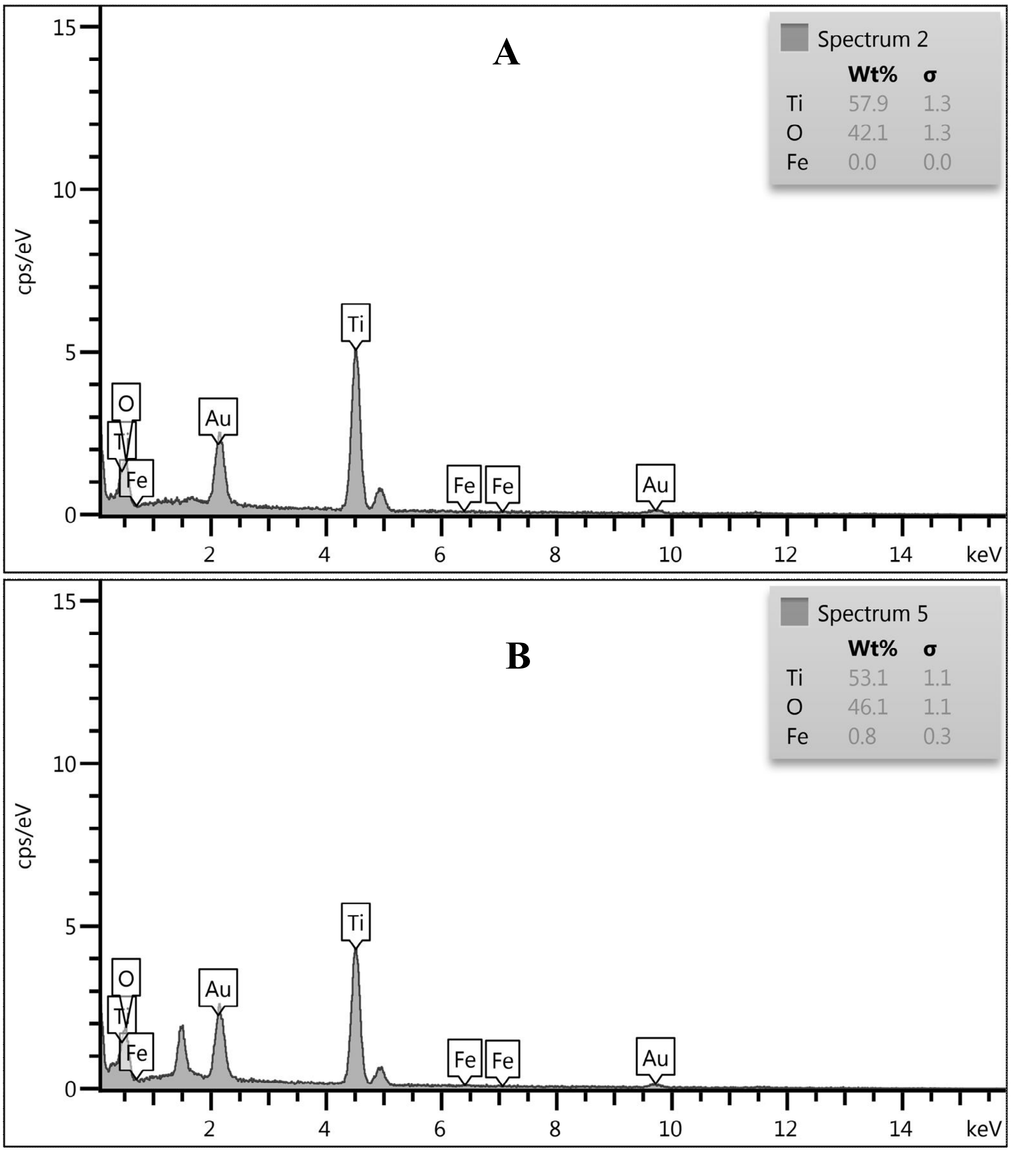

Fig. 4. EDX analyses of (A) pure and (B) 2% Fe-doped TiO_2 samples.

level, trapped by Fe^{3+} impurity, under the conduction band of Ti^{4+} causes a reduction in the recombination of the electron- holes pair and intensity of PL [28].

EDX Analysis

The EDX analysis was used to determine the elemental percentage in the sample. Figure 5 shows the x-ray energy diffraction (EDX) spectrum for pure and 2% Fe-doped TiO_2 samples. In the sample, the weight percentage of Ti measured was 57.9 wt% and 53.1 wt% for pure and Fe-doped samples, respectively. This difference in the percentages is due to the fact that in the EDX analysis, the Fe impurity has been entered into the TiO_2 matrix and replaced by Ti atoms.

CONCLUSIONS

Fe-doped TiO_2 nanocomposites were successfully prepared by the simple sol-gel precursors. The results were characterized by optical, morphological and structural analyzers. Based on the XRD results, the Fe-doped TiO_2 samples have the anatase phase with tetragonal structures and the crystallite size of about 29 nm. The surface morphology results from the FESEM analyzer showed a reduction in the distribution and homogeneity of the particles as Fe dopant increased to 2%. The UV-DRS results showed a red shift due to the reduction of the band gap caused by the existence of Fe content. Finally, PL analysis showed that the intensity of photoluminescence decreases for the Fe-doped sample.

REFERENCES

[1] Dastpak, M.; Farahmandjou, M.; Firoozabadi T. P., Synthesis and preparation of magnetic Fe-doped CeO_2 nanoparticles prepared by simple sol-gel method. *J. supercond Nov. Magn.* **2016**, *29*, 2925-2929, DOI: 10.1007/s10948-016-3639-3.

[2] Farahmandjou, M.; Honarbakhsh, S.; Behrouzinia, S., PVP-Assisted synthesis of cobalt ferrite ($CoFe_2O_4$) nanorods. *Phys. Chem. Res.* **2016**, *4*, 655-662, DOI: 10.22036/pcr.2016.16702.

[3] Farahmandjou, M.; Golabiyan, N., Synthesis and characterization of Alumina (Al_2O_3) nanoparticles prepared by simple sol-gel method. *Int. J. Bio-Inorg. Hybr. Nanomater. 2016, 5, 73-77.*

[4] Farahmandjou, M., The study of electro-optical properties of nanocomposite ITO thin films prepared by e-beam evaporation. *Rev. Mex. Fis.* **2013**, *59*, 205-207.

[5] Farahmandjou, M.; Golabiyan, N., Solution combustion preparation of nano-Al_2O_3: synthesis and characterization. *Transp. Phenom. Nano. Micro. Scales.* **2015**, *3*, 100-105.

[6] Akhtari, F.; Zoriasatain, S.; Farahmandjou, M.; Elahi, S. M., Synthesis and optical properties of Co^{2+}-doped ZnO Network prepared by new precursors. *Mater. Res. Express.* **2018**, *5*, 065015, DOI: 10.1088/2053-1591/aac6f1.

[7] Farahmandjou, M.; Motaghi, S., Sol-gel synthesis of Ce-doped α-Al_2O_3: Study of crystal and optoelectronic properties. *Opt. Commun.* **2019**, *441*, 1-7, DOI: 10.1016/j.optcom.2019.02.029.

[8] Farahmandjou, M.; Dastpak, M., Fe-Loaded CeO_2 nanosized prepared by simple Co-precipitation route. *Phys. Chem. Res.* **2018**, *6*, 713-720, DOI: 10.22036/pcr.2018.132220.1486.

[9] Khodadadi, A.; Farahmandjou, M.; Yaghoubi, M., Investigation on synthesis and characterization of Fe-doped Al_2O_3 nanocrystals by new sol-gel precursors. *Mater. Res. Express.* **2019**, *6*, 025029, DOI: 10.1088/2053-1591/aaef70.

[10] Motaghi, S.; Farahmandjou, M., Structural and optoelectronic properties of Ce-Al_2O_3 nanoparticles prepared by sol-gel precursors. *Mater. Res. Express.* 2019, *6*, 045008, DOI: 10.1088/2053-1591/aaf927.

[11] Lei, S.; Duan, W., Highly active mixed-phase TiO2 photocatalysts fabricated at low temperature and the correlation between phase composition and photocatalytic activity. *J. Environ. Sci. China.* **2008**, *20*, 1263-1267, DOI: 10.1016/S1001-0742(08)62219-6.

[12] Gang, L.; Xuewen, W.; Zhigang, C.; Hui-Ming, C.; Qing, L. G., The role of crystal phase in determining photocatalytic activity of nitrogen doped TiO_2. *Colloid Interface Sci.* **2009**, *329*, 331-338, DOI: 10.1016/j.jcis.2008.09.061.

[13] Farahmandjou, M.; Ramazani, M., Fabrication and characterization of rutile TiO_2 nanocrystals by water soluble precursor. *Phys. Chem. Res.* **2015**, *3*, 293-298, DOI: 10.22036/pcr.2015.10641.

[14] Farahmandjou, M.; Khalili, P., Study of nano SiO_2/TiO_2 superhydrophobic self-cleaning surface produced by sol-gel. *Aust. J. Basic. Appl. Sci.* **2013**, *7*, 462-465.

[15] Akhtari, F.; Zorriasatein, S.; Farahmandjou, M.; Elahi, S. M., Structural, optical, thermoelectrical, and magnetic study of Zn_1-xCo_xO ($0 \le x \le 0.10$) nanocrystals. *Int. J. Appl. Ceram. Technol.* **2018**, *15*, 723-733, DOI: 10.1111/ ijac.12848.

[16] Jurablu, S.; Farahmandjou, M.; Firoozabadi, T. P., Multiple-layered structure of obelisk-shaped crystalline nano-ZnO prepared by sol-gel route. *J. Theoretical. Appl. Phys.* **2015**, *9*, 261-266, DOI: 10.1007/s40094-015-0184-6.

[17] Wang, D.; Xiao, L.; Luo, Q.; Li, X.; An, J.; Duan, Y.,

Highly efficient visible light TiO_2 photocatalyst prepared by sol-gel method at temperatures lower than 300 °C. *J. Hazard. Mater.* **2011**, *192*, 150-159, DOI: 10.1016/j.jhazmat.2011.04.110.

[18] Zhang, Y.; Shen, Y.; Gu, F.; Wu, M.; Xie, Y.; Zhang, J., Influence of Fe ions in characteristics and optical properties of mesoporous titanium oxide thin films. J. *Appl. Surf. Sci.* **2009**, *256*, 85-89, DOI: 10.1016/j.apsusc.2009.07.074.

[19] Chiarello, G. L.; Selli, E.; Forni, L., Photocatalytic hydrogen production over flame spray pyrolysis-synthesised TiO_2 and Au/TiO_2. *Appl. Catal. B. Environ.* **2008**, *84*, 332-339, DOI: 10.1016/j.apcatb.2008.04.012.

[20] Li, L.; Zhuanga, H.; Bua, D., Characterization and activity of visible-light-driven TiO_2 photocatalyst codoped with lanthanum and iodine. *Appl. Surf. Sci.* **2011**, *257*, 9221-9225, DOI: 10.1016/j.apsusc.2011.06.007

[21] Li, Z.; Shen, W.; Hea, W.; Zu. X., Effect of Fe-doped TiO2 nanoparticle derived from modified hydrothermal process on the photocatalytic degradation performance on methylene blue. *J. Hazard. Mater.* **2008**, *155*, 590-594, DOI: 10.1016/j.jhazmat.2007.11.095.

[22] Khoshnevisan, B.; Marami, M. B.; Farahmandjou, M., Fe^{3+}-Doped Anatase TiO_2 Study prepared by new sol-gel precursors. *Chin. Phys. Lett.* **2018**, *35*, 027501, DOI: 10.1088/0256-307X/35/2/027501.

[23] Khoshnevisan, B.; Marami, M. B.; Farahmandjou, M., Solgel synthesis of Fe-doped TiO_2 nanocrystals. J. electron. *Mater.* **2018**, *47*, 3741-3749, DOI: 10.1007/s11664-018-6234-5.

[24] Scherrer, P., Bestimmung der grosse und der inneren struktur von kolloidteilchen mittels rontgenstrahlen, nachrichten von der gesellschaft der wissenschaften. *Gottingen. Mathematisch-Physikalische Klasse.* **1918**, *2*, 98-100, DOI: 10.4236/health.2011.37070 2.486.

[25] Chen, Q.; Xue, C.; Li, X.; Wang, Y., Surfactants Effect on the Photoactivity of Fe-Doped TiO_2. *Mater. Sci. Forum.* **2013**, *743*, 367-371, DOI: 10.4028/www.scientific.net/MSF.743-744.367.

[26] Farahmandjou, M., Effect of oleic acid and oleylamine surfactants on the size of FePt nanoparticles. *J. Supercond. Nov. Magn.* **2012**, *25*, 2075-2079, DOI: 10.1007/s10948-012-1586-1

[27] Khatoon, S.; Wani, I. A.; Ahmed, J.; Magdaleno, T.; Al-Hartomy, O. A.; Ahmad, T., Effect of high manganese substitution at ZnO host lattice using solvothermal method: Structural characterization and properties. *Mater. Chem. Phys.* **2013**, *138*, 519-528, DOI: 10.1016/j.matchemphys.2012.12.013.

[28] Abazovic, N. D.; Comor, M. I.; Dramicanin, M. D.; Jovanovic, D. J.; Ahrenkiel, S. P.; Nedeljkovic, J. M., Photoluminescence of anatase and rutile TiO_2 particles. *J. Phys. Chem. B.* **2006**, *110*, 25366-25370, DOI: 10.1021/jp064454f.